Glutathione/thioredoxin systems modulate mitochondrial H_2O_2 emission: An experimental-computational study

Miguel Antonio Aon, Brian Alan Stanley, Vidhya Sivakumaran, Jackelyn Melissa Kembro, Brian O'Rourke, Nazareno Paolocci, and Sonia Cortassa

Division of Cardiology, Johns Hopkins University School of Medicine, Baltimore, MD 21205

The net emission of hydrogen peroxide (H_2O_2) from mitochondria results from the balance between reactive oxygen species (ROS) continuously generated in the respiratory chain and ROS scavenging. The relative contribution of the two major antioxidant systems in the mitochondrial matrix, glutathione (GSH) and thioredoxin (Trx), has not been assessed. In this paper, we examine this key question via combined experimental and theoretical approaches, using isolated heart mitochondria from mouse, rat, and guinea pig.

As compared with untreated control mitochondria, selective inhibition of Trx reductase with auranofin along with depletion of GSH with 2,4-dinitrochlorobenzene led to a species-dependent increase in H_2O_2 emission flux of 17, 11, and 6 fold in state 4 and 15, 7, and 8 fold in state 3 for mouse, rat, and guinea pig mitochondria, respectively. The maximal H_2O_2 emission as a percentage of the total O_2 consumption flux was 11%/2.3% for mouse in states 4 and 3 followed by 2%/0.25% and 0.74%/0.29% in the rat and guinea pig, respectively.

A minimal computational model accounting for the kinetics of GSH/Trx systems was developed and was able to simulate increase in H_2O_2 emission fluxes when both scavenging systems were inhibited separately or together. Model simulations suggest that GSH/Trx systems act in concert. When the scavenging capacity of either one of them saturates during H_2O_2 overload, they relieve each other until complete saturation, when maximal ROS emission occurs.

Quantitatively, these results converge on the idea that GSH/Trx scavenging systems in mitochondria are both essential for keeping minimal levels of H_2O_2 emission, especially during state 3 respiration, when the energetic output is maximal. This suggests that the very low levels of H_2O_2 emission observed during forward electron transport in the respiratory chain are a result of the well-orchestrated actions of the two antioxidant systems working continuously to offset ROS production.

INTRODUCTION

Reactive oxygen species (ROS) are continuously produced by respiring mitochondria, and their level greatly depends on the mode of electron transport in the respiratory chain. Forward mode of electron transport (forward electron transport [FET]) and reverse mode of electron transport can be elicited by substrates of complex I (e.g., glutamate and malate) and complex II (e.g., succinate), respectively (Schönfeld and Wojtczak, 2008). The former represents the main in vivo physiological pathway of electron flow.

Mitochondria produce ∼85–90% of cellular ROS (Chance et al., 1979; Balaban et al., 2005). Sources of ROS other than the respiratory chain include mitochondrial nicotinamide adenine dinucleotide phosphate (NADPH) oxidase (NOX4; Bedard and Krause, 2007; Kuroda et al., 2010), α-ketoglutarate dehydrogenase (Starkov et al., 2004), glycerol 3-phosphate dehydrogenase (Andreyev et al., 2005; Adam-Vizi and Chinopoulos, 2006), monoamine oxidase (Kaludercic et al., 2010), and several others (Andreyev et al., 2005; Murphy, 2009).

Separate, but interacting, pools of the main redox couples (NADH/NAD^+, GSH [reduced glutathione]/GSSG [oxidized glutathione], $Trx(SH)_2$ [reduced Trx]/TrxSS [oxidized Trx], and NADPH/$NADP^+$) are present in the cytoplasm, mitochondrial intermembrane space (IMS), and matrix (Aon et al., 2007; Go and Jones, 2008; Hu et al., 2008). Redox sensors in cytoplasmic and mitochondrial compartments are capable of dynamic and rapid detection of changes in ROS levels, tuning the antioxidant defenses to respond to intra- or extracellular redox stressors that may perturb mitochondrial and cytosolic redox balance (Aon et al., 2007, 2010a; Drechsel and Patel, 2010; Sheeran et al., 2010).

The H_2O_2 emission flux from mitochondria reflects the balance between the rate of H_2O_2 generation, secondary to superoxide production by the respiratory chain and its dismutation to H_2O_2, and the rate of

Correspondence to Sonia Cortassa: scortas1@jhmi.edu

Abbreviations used in this paper: AF, auranofin; DNCB, dinitrochlorobenzene; FET, forward electron transport; IMS, intermembrane space; NADPH, nicotinamide adenine dinucleotide phosphate; ROS, reactive oxygen species; SOD, superoxide dismutase.

The Rockefeller University Press $30.00
J. Gen. Physiol. Vol. 139 No. 6 479–491
www.jgp.org/cgi/doi/10.1085/jgp.201210772

H_2O_2 scavenging (Andreyev et al., 2005; Kowaltowski et al., 2009; Murphy, 2009; Stowe and Camara, 2009; Aon et al., 2010a). Superoxide dismutation to H_2O_2 is accomplished primarily by Mn (mitochondrial matrix), Cu, and Zn (cytoplasmic and mitochondrial IMS) superoxide dismutases (SODs), enzymes with very high rate constants, on the order of 800 $\mu M\ s^{-1}$ (Chockalingam et al., 2006). Superoxide can also be oxidized to O_2 independently of SOD by oxidized cytochrome c (rate constant of $\sim$1–10 $\mu M\ s^{-1}$; Butler et al., 1982) residing in the IMS (Korshunov et al., 1999; Han et al., 2001; Pasdois et al., 2011), although it has been argued that cytochrome c must first be released from the inner membrane before it can serve as an antioxidant (Pereverzev et al., 2003).

The glutathione (GSH) and Trx systems are the two main H_2O_2 scavengers that have been characterized in mitochondria from all organs. In the mitochondrial matrix, the Trx system is composed of Trx reductase 2 (TrxR2), Trx2, and peroxiredoxin 3 (Prx3). The GSH system encompasses the activities of glutathione reductase (GR) and glutathione peroxidase (GPx). The cytoplasmic TrxR1 (Iñarrea et al., 2007) and other cytoplasmic antioxidants, such as the GSH system (Hu et al., 2008), Cu, Zn SOD (SOD1), and catalase (Iñarrea et al., 2007), have also been found in the mitochondrial IMS.

The mitochondrial H_2O_2 buffering capacity maintains proper reduced/oxidized ratios of GSH and Trx pools as the result of their constitutive enzymatic activities (Kowaltowski et al., 2009; Murphy, 2009; Stowe and Camara, 2009). Trx2/TrxR2 does not directly scavenge H_2O_2 but instead supplies electrons to Prx3 (Pérez et al., 2008; Cox et al., 2010; Holmgren and Lu, 2010). In doing so, Trx2 shifts from a reduced to oxidized form. The activity of both systems, Trx2 and GSH, is dependent on the electron donor NADPH, whose reductive potential in the mitochondrial matrix is set by the activity of the nicotinamide nucleotide transhydrogenase, $NADP^+$-dependent isocitrate dehydrogenase, and malic enzyme (Sazanov and Jackson, 1994; Rydström, 2006).

The physiological importance of the balance between ROS production and scavenging is underscored by observations in several diseases that ROS can be either protective or damaging (Camara et al., 2011). Diabetes and insulin resistance are associated with decreased antioxidant capacity, reflected as diminished activities of SOD, GPx, and GR (Styskal et al., 2012). Under redox-balanced conditions, H_2O_2 production is offset by matrix peroxidases, including Prx3 and Prx5 (Rhee et al., 2001; Cox et al., 2010), catalase (Radi et al., 1991; Salvi et al., 2007), and GPx1 and 4 (Imai and Nakagawa, 2003). The cytoplasmic and mitochondrial redox environments play an important role in maintaining ROS balance within cardiac myocytes. Cellular and mitochondrial ROS levels are highly responsive to matrix and extramitochondrial scavenging systems. The Redox-optimized ROS Balance hypothesis postulates that oxidative stress can occur at either extreme of the redox potential range, that is, when the intracellular environment is either highly reduced or oxidized (Aon et al., 2010a). Previously, we have shown that in permeabilized cardiomyocytes and mitochondria isolated from guinea pig hearts, the rate of ROS accumulation depends on the interplay between extramitochondrial GSH/GSSG ratio and GSH regeneration in the mitochondrial matrix (Aon et al., 2007, 2010a). At sufficiently oxidized redox environments, the antioxidant defense systems determine the extent of ROS imbalance, which may result in mitochondrial dysfunction and contribute to contractile impairment and whole-heart arrhythmias (Aon et al., 2006, 2009; Slodzinski et al., 2008; Brown et al., 2010; Biary et al., 2011).

In the present study, we quantitatively analyzed, by means of experimentation and computational modeling, the relative contribution of the two main antioxidant arms (GSH and Trx1/2) in modulating mitochondrial H_2O_2 emission (Fig. 1). Auranofin (AF) and dinitrochlorobenzene (DNCB) were used to quantitatively characterize the contribution of each system separately and when acting together to scavenge H_2O_2. We combined experimental and modeling results to understand in quantitative terms the relative weight of the two major antioxidant systems in preventing H_2O_2 emission from mitochondria. Our investigation was performed in isolated heart mitochondria from mouse, rat, and guinea pig, three species that are widely used in cardiovascular science and have different electrophysiological and contractile properties. We also aimed at assessing whether differences related with the aims of this study exist between species that exhibit different maximum life span potential (4, 5, and 12 yr for mouse, rat, and guinea pig, respectively; Barja, 1998). This important aspect of our choice was stimulated by the well-established negative correlation found between mitochondrial ROS and maximum life span potential (Sanz et al., 2009). Overall, studying mitochondria from several distinct species allowed us to further ascertain the general validity of the results obtained.

MATERIALS AND METHODS

Mitochondrial isolation

Procedures for the isolation and handling of mitochondria from guinea pig and rat hearts were performed as previously described (Aon et al., 2010a,b). Mitochondria from two pooled mouse hearts were isolated, with slight modifications, as described in Stanley et al. (2011). In brief, 0.1mg/ml proteinase (bacterial, type XXIV, formerly called Nagarse; Sigma-Aldrich) was added immediately before the homogenization procedure (Aon et al., 2010b). 3 vol of isolation solution (75 mM sucrose, 225 mM mannitol, and 1 mM EGTA, pH 7.4, containing 0.2% fatty acid–free BSA; Sigma-Aldrich) was quickly added after homogenization to block proteinase

activity. After a first centrifugation (500 *g* for 10 min) to discard unbroken tissue and debris, the supernatant was centrifuged at 10,000 *g* for 10 min to sediment the mitochondria and washed twice thereafter by centrifugation at 7,700 *g* for 5 min each, the first one with isolation solution in presence of BSA and the second in absence of BSA. In mouse heart mitochondria, respiratory control ratios (state 3/state 4 respirations with 5 mM glutamate + malate or succinate) of five or higher were obtained using this method.

Assay of mitochondrial respiration

Respiration was assayed in freshly isolated mitochondria with a high-throughput–automated 96-well extracellular flux analyzer (XF96; Seahorse Bioscience) in a medium (buffer B) containing 137 mM KCl, 2 mM KH_2PO_4, 0.5 mM EGTA, 2.5 mM $MgCl_2$, and 20 mM HEPES at pH 7.2 and 37°C in presence of 0.2% fatty acid–free BSA. Respiration was evaluated with substrates of complex I (glutamate/malate [G/M], 5 mM each). The day before the experiment, each of the 96 wells of the XF96 plate was coated with 120 µl polyethylenimine (1:15,000 dilution in buffer B of a 50% solution of polyethylenimine) and incubated overnight in the absence of CO_2. The next day, the solution of polyethylenimine was removed by vacuum suction. After transferring appropriate amounts of mitochondrial suspension into each well (5–15 µg of mitochondrial protein), the mitochondria were spun down at 3,000 *g* for 7 min at 4°C in a centrifuge with a swinging bucket rotor (S5700; Beckman Coulter) with a microplate adaptor. After centrifugation, the plate was incubated at 37°C for 20 min before starting the assay in the Seahorse Bioscience equipment. Mitochondrial protein was determined using the bicinchoninic acid method protein assay kit (Thermo Fisher Scientific).

Other bioenergetic variables and ROS detection

NAD(P)H and H_2O_2 were determined, as previously described (Aon et al., 2010a,b), and monitored simultaneously with a wavelength-scanning fluorometer (QuantaMaster; Photon Technology International, Inc.) using the same aforementioned medium for measuring respiration (excluding BSA) and a multidye program for simultaneous online monitoring of different fluorescent probes. NAD(P)H was monitored by exciting mitochondrial suspensions at 340 nm and collecting the emission at 450 nm. H_2O_2 was detected using the Amplex red kit (Invitrogen).

Computational model formulation

A minimal model of mitochondrial ROS scavenging accounting for the GSH and Trx systems was formulated, taking into account kinetic information available (see scheme in Fig. 4 A). The rate expressions used in the model were formulated as follows. Eqs. 1 and 2 correspond to the same expressions used in our mitochondrial model of ROS metabolism (Cortassa et al., 2004):

$$V_{GPx} = \frac{E^T_{GPX}\ [H_2O_2]\ [GSH]}{\Phi_1[GSH] + \Phi_2\ [H_2O_2]} \quad (1)$$

and

$$V_{GR} = \frac{k^1_{GR}\ E^T_{GR}\ [GSSG]\ [NADPH]}{[GSSG]\ [NADPH] + K^{GSSG}_M\ [NADPH] + K^{NADPH}_M\ [GSSG] + K^{GSSG}_M\ K^{NADPH}_M}. \quad (2)$$

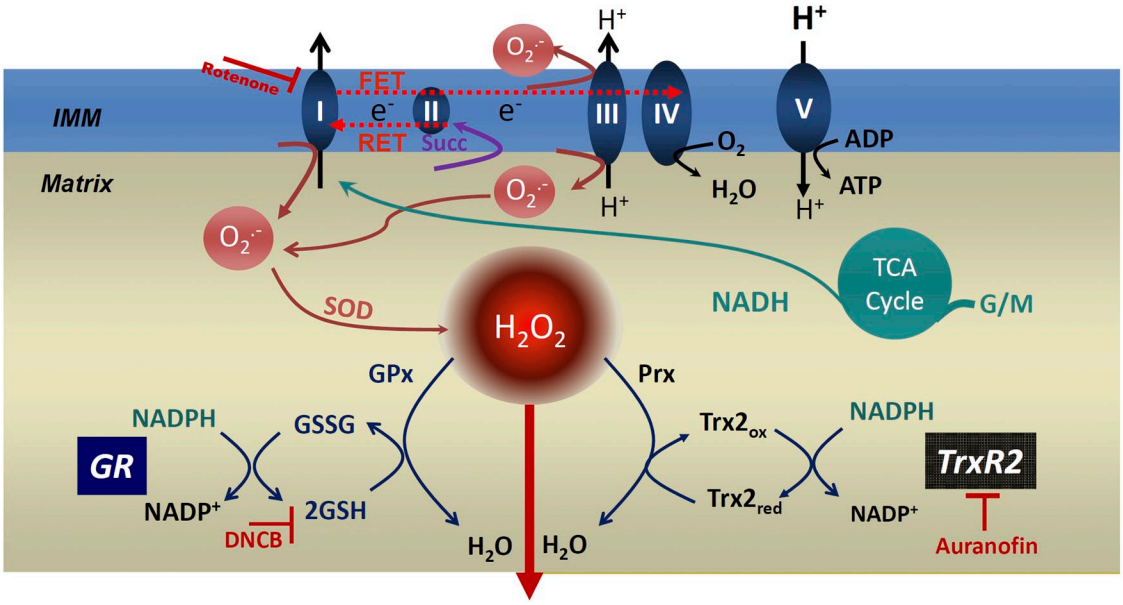

Figure 1. Major pathways of mitochondrial ROS production and ROS scavenging. The scheme depicts the GSH and Trx systems in the mitochondrial matrix as the major H_2O_2 scavengers. The NADPH/$NADP^+$ couple is the main electron donor of the large-capacity GSH (GSH and GSSG) and the Trx (Trx_{red} and Trx_{ox}) systems responsible for scavenging H_2O_2 via GPx and Prx enzymes, respectively. GR and TrxR, the two reductases responsible for regenerating the reduced species of both antioxidant defenses, GSH and Trx_{red}, are shown. The two inhibitors used in this work and their sites of action are highlighted: AF, the TrxR1/2 inhibitor, and DNCB, an alkylating GSH-depleting agent. The respiratory complexes I, II, III, IV, and V (ATP synthase) in the inner mitochondrial membrane (IMM) are also schematized. O_2^- can be produced by complexes I and III from the electron transport chain through reverse electron transport (RET) or FET (reverse or forward modes of electron transport), which depends on NADH- or flavin adenine dinucleotide hydrogen–linked substrates, such as G/M or succinate (Succ), donating electrons to complex I or II, respectively. O_2^- conversion to H_2O_2 by Mn SOD and the tricarboxylic acid (TCA) cycle are depicted as well. In the scheme of the computational model (see Fig. 4 A), we have split the arrow corresponding to Prx into two processes to account for the cycle of Prx oxidation/reduction as well. These processes are denoted by V_{Prx} and V_{txpx} (Eqs. 3 and 5; see Computational model formulation in Materials and methods).

Eq. 3 was derived on the basis of the experimental studies performed by Sztajer et al. (2001), from which we also obtained the rate constants:

$$V_{Prx} = \frac{E^{T}_{PrxX}\ [H_2O_2]\ [Prx(SH)_2]^2}{\Phi_{P1}\ [Prx(SH)_2] + \Phi_{P2}\ [H_2O_2]}. \quad (3)$$

Eq. 4 represents a Michaelis–Menten rate expression with two substrates (NADPH and TrxSS), with kinetic parameters derived from Pillay et al. (2009) and Eckenroth et al. (2006):

$$V_{TrxR} = \frac{k^{1}_{TrxR}\ E^{T}_{TrxR}\ [Trx(SS)]\ [NADPH]}{[Trx(SS)]\ [NADPH] + K_M^{TrxSS}\ [NADPH] + K_M^{T\text{-}NADPH}\ [Trx(SS)] + K_M^{TrxSS}\ K_M^{T\text{-}NADPH}}. \quad (4)$$

The rate expression of Prx oxidation (Eq. 5) was based on the model of Pillay et al. (2009), with adjustable k_{txpx} to simulate the results obtained with heart mitochondria:

$$V_{TxPx} = \frac{k^{1}_{TxPx}\ [Trx(SH)_2]\ [Prx(SS)]}{[Trx(SH)_2] + K_M^{Trx} + K_i^{TrxPx}\ [Trx(SH)_2]^2}. \quad (5)$$

The model contains the following components: (a) TrxR and reduced Prx ($Prx(SH)_2$)as part of the Trx system, present in both matrix and IMS, which considers the reduced/oxidized species of Trx and Prx as state variables (both couples linked through conservation relationships); and (b) the GSH system, encompassing the activities of GPx and GR, with GSH/GSSG as state variables, also obeying conservation relations. In the present model, catalase was not taken into account because very low concentrations have been detected in heart mitochondria (Radi et al., 1991) and because we did not observe effects on H_2O_2 emission after its inhibition, under the same experimental conditions used in this work (Stanley et al., 2011).

In keeping with the main aim of the present work, which was to quantify the role of the GSH/Trx scavenging systems in controlling ROS emission from mitochondria, the following basic questions prompted the use of modeling: (a) are the basic biochemical mechanisms involved in the GSH/Trx scavenging systems sufficient to quantitatively explain the experimentally measured H_2O_2 emission fluxes; (b) how do the two scavenging systems behave kinetically when acting together with respect to H_2O_2 scavenging; and (c) is another mechanism needed in the model formulation to account for the observed behavior of H_2O_2 emission when both systems are inhibited, either independently or in tandem?

In this minimal model, the rate of H_2O_2 generation and the concentration of NADPH are adjustable parameters. The input given by the rate of H_2O_2 generation represents the activity of SOD (V_{SOD}). The rate equations of the individual processes (Eqs. 1–5) have been integrated into a system of four ordinary differential equations (see Table 1). The concentrations of the redox couples GSH/GSSG, $Trx(SH)_2$/Trx(SS), and $Prx(SH)_2$/Prx(SS) (oxidized Prx) are related through conservation relations (Eqs. 6–8):

$$G_T = [GSH] + 2\,[GSSG], \quad (6)$$

$$Trx_T = [Trx(SH)_2] + [Trx(SS)], \quad (7)$$

and

$$Prx_T = [Prx(SH)_2] + [Prx(SS)]. \quad (8)$$

The ordinary differential equation system was numerically integrated with MATCONT (Dhooge et al., 2008) both for time-dependent behavior and continuation analysis of the steady state as a function of the model parameters. Mathematically, the rate expressions and their parameters were formulated according to reported experimental data (see Table 2).

Online supplemental material

This section presents additional experimental and modeling data. Fig. S1 displays representative traces of H_2O_2 emission obtained at different doses of AF or DNCB inhibition of the antioxidant defenses that are summarized in Fig. 2. Fig. S2 shows the steady-state behavior of the computational model as a function of the parameter representing the NADPH concentration. Online supplemental material is available at http://www.jgp.org/cgi/content/full/jgp.201210772/DC1.

RESULTS

Kinetics of H_2O_2 emission flux from mitochondria upon inhibition of either the GSH or Trx system

We measured respiratory and H_2O_2 emission fluxes in parallel from mitochondria isolated from mouse, rat, and guinea pig hearts. As FET corresponds to the physiological mode of electron transport in the respiratory chain, we measured respiration in the presence of NADH-linked substrates (G/M, 5 mM each) without (state 4) or with (state 3) 1 mM ADP.

Two inhibitors, AF and DNCB, were used to selectively and equally inhibit, in the matrix and IMS, the Trx1/2 and GSH systems, respectively (Stanley et al., 2011). The main rationale underlying our approach was that the increase in ROS emission observed in respiring mitochondria in the presence of each individual inhibitor represents the amount of H_2O_2 being scavenged by that antioxidant system, assuming that the respiratory chain is the main supplier of ROS, Mn SOD is not rate controlling, and both GSH and Trx1/2 are the main scavenging systems in the mitochondrial matrix and IMS. Hence, the simultaneous blockade of both should render the maximum percentage of the total O_2 consumption flux being diverted to ROS generation. Knowing the total increase in H_2O_2 emission

TABLE 1

Model differential equations

State variable	Differential equation
$[H_2O_2]$	$\frac{d[H_2O_2]}{dt} = V_{SOD} - k_1 \times [H_2O_2] - V_{Prx} - V_{GPx}$
[GSH]	$\frac{d[GSH]}{dt} = V_{GR} - V_{GPx}$
$[Trx(SH)_2]$	$\frac{d[Trx(SH)_2]}{dt} = V_{TrxR} - V_{TxPx}$
$[Prx(SH)_2]$	$\frac{d[Prx(SH)_2]}{dt} = V_{TxPx} - V_{Prx}$

obtained at maximal inhibition with both AF and DNCB, we can calculate (in percentage) the extent of scavenging performed by each system.

To choose the appropriate concentration of the inhibitor, we performed dose-response curves for AF and DNCB while monitoring H_2O_2 emission in mitochondria respiring under FET in states 4 and 3. The results are shown in Fig. 2 for mouse (Fig. 2 A), rat (Fig. 2 B), and guinea pig (Fig. 2 C) mitochondria. Representative traces of the dynamics of H_2O_2 emission during state 4 and 3 respiration as a function of the inhibitor concentrations are shown in Fig. S1. The maximal AF-elicited H_2O_2 fluxes obtained from mouse, rat, and guinea pig mitochondria under states 4/3 (Fig. 2, A–C [left graphs]) are summarized in Table 3. DNCB produced larger H_2O_2 fluxes from mouse and rat mitochondria in comparison with AF but similar ones in guinea pig (Fig. 2, A–C [right graphs]; Table 3). Also summarized in Table 3 are the $K_{0.5}$ inhibitory constants (dose of compound producing 50% of maximal H_2O_2 emission) by AF and DNCB in states 4/3 obtained from data in Fig. 2. Overall, the GSH-depleting agent increased H_2O_2 emission with a $K_{0.5}$ approximately three orders of magnitude higher than the TrxR2 inhibitor for the mouse (0.95 µM vs. 1.32 nM) and two orders of magnitude for rat and guinea pig (1–2 µM vs. 3–15 nM). The H_2O_2 emission levels in the presence of each inhibitor differed according to species, likely reflecting a different participation of GSH and Trx systems in H_2O_2 scavenging.

H_2O_2 emission as a percentage of the total O_2 consumption flux

We then asked whether the continuous and concerted action of both scavenging systems was masking a higher flux of ROS production from the respiratory chain. To test this point, we applied both AF and DNCB together at concentrations (50 nM and 10 µM, respectively) that produce maximal H_2O_2 emission in all species analyzed. The total ROS flux as a percentage of the respiratory flux was determined from parallel measurements of O_2 consumption and H_2O_2 emission in the same mitochondrial preparation from the three species.

The results obtained after maximal inhibition of the GSH and Trx1/2 systems are depicted in Table 4. The findings suggest that the low H_2O_2 emission observed under FET in both respiratory states 4 and 3 is a result of the continuous scavenging action by GSH and Trx1/2. For instance, the flux of H_2O_2 emission from rat mitochondria after complete inhibition of GSH and Trx1/2 systems under FET (in nmol H_2O_2 min^{-1} mg^{-1} protein) is 1.16 and 0.55, whereas the respiratory flux, VO_2 (nmol min^{-1} mg^{-1} protein), under the same conditions is 35 and 202 in states 4 and 3, respectively. We calculated that

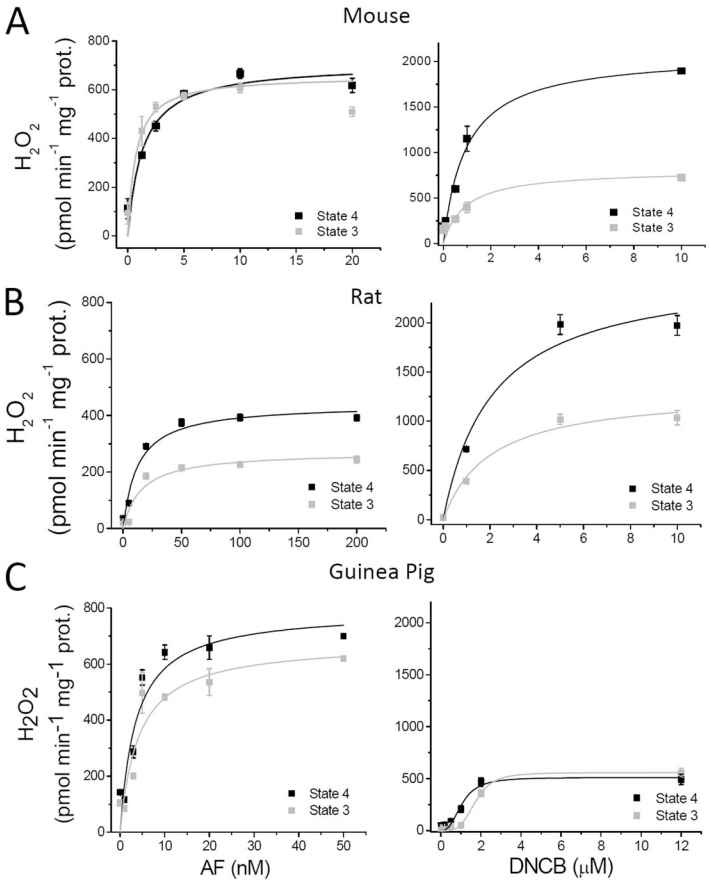

Figure 2. Effect of AF or DNCB on H_2O_2 emission from heart mitochondria under FET at states 4 and 3 of respiration. (A–C) Freshly isolated mitochondria (~100 µg mitochondrial protein [prot.]) from mouse, rat, and guinea pig hearts were preincubated in the absence or the presence of the indicated concentrations of AF (left graphs) or DNCB (right graphs) in the presence of the NADH-linked substrates G/M (5 mM each). Monitoring of H_2O_2 was performed with the Amplex red assay during states 4 (with G/M) and 3 (+1 mM ADP) of mitochondrial respiration (Stanley et al., 2011). The specific fluxes of H_2O_2 emission are shown. The kinetic parameters describing the fluxes of H_2O_2 emission as a function of the inhibitor concentration, V_{max} and $K_{0.5}$, were determined after nonlinear regression fitting of the experimental points with a hyperbolic Michaelis–Menten or Hill type of equation. The results ± SEM obtained from two experiments with duplicates in each are represented.

TABLE 2

Parameter values of the computational model

Symbol	Value	Unit	Description	Equation no.	Reference
E_{GPX}^{T}	5.0×10^{-3}	mM	Mitochondrial concentration of GPx	1	Cortassa et al., 2004
Φ_1	5.0×10^{-3}	mM ms	Constant for GPx activity	1	Cortassa et al., 2004
Φ_2	0.75	mM ms	Constant for GPx activity	1	Cortassa et al., 2004
K_M^{GSSG}	0.06	mM	K_m for oxidized GSH of GR	2	Cortassa et al., 2004
K_M^{NADPH}	0.015	mM	K_m for NADPH of GR	2	Cortassa et al., 2004
k_{GR}^{1}	0.025–0.005	ms^{-1}	Rate constant of GR	2	Cortassa et al., 2004
E_{GR}^{T}	5.0×10^{-3}	mM	Mitochondrial concentration of GR	2	Cortassa et al., 2004
G_T	3.0	mM	Total mitochondrial pool of GSH	6	Cortassa et al., 2004
E_{PrxX}^{T}	1	mM	Intracellular concentration of Prx	3	Cox et al., 2010
Φ_{P1}	3.83	mM^2 ms	Constant for Prx 3 activity	3	Sztajer et al., 2001
Φ_{P2}	0.285	mM^2 ms	Constant for Prx 3 activity	3	Sztajer et al., 2001
K_M^{TrxSS}	0.05	mM	K_m for Trx(SS) of TrxR	4	Pillay et al., 2009; Eckenroth et al., 2006
$K_M^{T-NADPH}$	0.012	mM	K_m for NADPH of TrxR	4	Pillay et al., 2009; Eckenroth et al., 2006
k_{TrxR}^{1}	0.022–0.009	ms^{-1}	Rate constant of TrxR	4	Pillay et al., 2009; Eckenroth et al., 2006
E_{TrxR}^{T}	0.025	mM	Mitochondrial concentration of TrxR	4	Pillay et al., 2009
k_{TxPx}^{1}	2.5	mM^{-1} ms^{-1}	Rate constant of Prx	5	Cox et al., 2010; Adimora et al., 2010
K_M^{Trx}	0.1	mM	K_m for $Trx(SH)_2$ of Prx	5	Adimora et al., 2010
K_i^{TrxPx}	0.01	mM^{-1}	Inhibition constant of Prx activity by $Trx(SH)_2$	5	Adimora et al., 2010
Trx_T	0.025	mM	Total mitochondrial pool of Trx	7	Cox et al., 2010
Prx_T	0.15	mM	Total mitochondrial pool of Prx	8	Cox et al., 2010
k_1	0.1	ms^{-1}	Rate constant of H_2O_2 transport from mitochondria	9	Adjusted[a]

[a]This parameter (k_1) was adjusted.

the H_2O_2 emission represents 2 and 0.25% of the total O_2 consumption flux in rat heart mitochondria under states 4 and 3, respectively. Data for mouse and guinea pig are also analyzed in Table 4, where it can be appreciated that mitochondria from both species represent two extreme situations. In mouse mitochondria, H_2O_2 emission represents 11 and 2.3% of the total O_2 consumption in states 4 and 3, respectively, whereas in guinea pig, H_2O_2 rates amounted to only 0.7 and 0.3%.

In all cases, state 4 displayed a higher percentage of ROS emission than state 3, with respect to respiration. However, it is worth noting that in state 3, the relative impact of mitochondrial antioxid ant system inhibition is greater than previously recognized in terms of controlling ROS emission (Table 4). To quantify this novel observation, we calculated the extent to which the H_2O_2 emission flux was originally underestimated under FET in the absence of inhibitors. For example, mouse

TABLE 3

Kinetics of H_2O_2 emission from mitochondria under FET in the absence or presence of inhibitors

Condition		Mouse		Rat		Guinea pig	
		State 4	State 3	State 4	State 3	State 4	State 3
H_2O_2 emission[a]	Control	107 ± 1.5	82 ± 1.5	105 ± 2.5	80 ± 5	95 ± 3	62 ± 3
	+AF	707 ± 65	585 ± 49	440 ± 29	271 ± 30	791 ± 92	678 ± 91
	+DNCB	2085 ± 195	767 ± 165	2541 ± 210	1309 ± 144	512 ± 47	558 ± 31
$K_{0.5}$	AF (nM)	1.32 ± 0.5	0.4 ± 0.2	12.5 ± 3.7	15 ± 7	3.5 ± 1.5	4.1 ± 1.9
	DNCB (μM)	0.95 ± 0.27	0.8 ± 0.5	2.1 ± 0.4	2.0 ± 0.76	1.05 ± 0.16	1.7 ± 0.12

[a]H_2O_2 emission in all cases is expressed in pmol min^{-1} mg^{-1} protein.

mitochondria in state 4 emit 1% of VO_2 as H_2O_2; however, in the presence of maximal inhibition, this increased 11 fold to 11%. Similarly, in all three species, the original values of H_2O_2 emitted per O_2 consumed were underestimated between 4 and 11 fold under state 4 and from 6 to 13 fold under state 3 respiration (Table 4).

The doses of inhibitors used to obtain the data shown in Table 4 were further tested to determine the effects exerted by AF and DNCB alone or together on VO_2. In Fig. 3, we show the results obtained with mitochondria from guinea pig heart. The addition of either inhibitor alone had no effect on state 4 or state 3 respiration (Fig. 3, A and B). However, when added together, AF and DNCB significantly increased state 4 (~60%) and only slightly increased (10%) state 3 respiration. These effects were taken into account in the values shown in Table 4.

Additionally, we tested the effects of the inhibitors given individually, or in combination, on NADH levels while simultaneously monitoring H_2O_2 emission. Other than increasing H_2O_2 flux from mitochondria (Fig. 2), AF and DNCB, individually or together, had no significant impact on the mitochondrial NADH response (normalized to the initial NADH fluorescence) upon substrate addition (G/M and ADP; Fig. 3 C). However, before substrate addition, the NADH pool was more oxidized (~50%) in mitochondria preincubated with both inhibitors, consistent with the higher NADH oxidation rate indirectly indicated by the higher state 4 respiration (Fig. 3 A). Collectively the results depicted in Figs. 2 and 3 and additional data (not depicted) indicate that the behavior of the three species analyzed was similar.

Computational modeling of the Trx and GSH scavenging systems

To better understand the dynamics of the concerted action of the GSH/Trx systems in mitochondria, we formulated a minimal model accounting for the known kinetics of the two systems. Fig. 4 A schematically depicts the processes taken into account (see Computational model formulation in Materials and methods). In this model scheme, the arrow pointing to H_2O_2 emission, V_{H2O2} emission, is in fact the resultant of the supply of H_2O_2 by V_{SOD} minus the consumption exerted by the two scavenging systems, which at the steady state can be written as follows:

$$V_{H_2O_2 emission} = V_{SOD} - V_{GPx} - V_{Prx}.$$

The behavior of the model was studied as a function of the activity of V_{SOD} and for various combinations of the maximal rates of GSH and Trx subsystems varied through the catalytic rate constants of GR and TrxR.

A parametric condition representing a relative catalytic ratio of GR to TrxR of two was able to mimic the proportion contributed by each system to the scavenging observed experimentally. Fig. 4 B shows the plot of the rates of GPx, TrxR, and V_{H2O2} emission and the concentrations of $Trx(SH)_2$ and GSH when the system is challenged with increasing H_2O_2 input (V_{SOD}). The GSH system reached its maximal capacity at lower V_{SOD}, as indicated by the consumption of GSH and the observed plateau of GPx activity. The TrxR system increased its rate upon saturation of the GSH system along with the rate of H_2O_2 emission. The maximal V_{H2O2} emission was attained after the H_2O_2 production exceeded the sum of the two scavenging systems, after which H_2O_2 emission increased almost proportionally with V_{SOD}.

Model simulations show the time-dependent increase in V_{H2O2} when both scavenging systems are inhibited simultaneously (Fig. 4 C) or independently (Fig. 5, A and B). When simultaneously inhibited, loss of control over V_{H2O2} occurs only after both GSH and $Trx(SH)_2$ are completely consumed, recapitulating the experimental observations under the same conditions (Fig. 4 C). In fact, the 17-fold increase obtained in the simulation is comparable with the values reported in Table 4 for

TABLE 4

Quantitation of respiration, H_2O_2 emission, and electron flow diversion to ROS in isolated heart mitochondria from three different species

	VO_2		H_2O_2 emission[a]		Respiratory flux as H_2O_2 emission[b]	
	State 4	State 3	State 4	State 3	State 4	State 3
	nmol/min/mg	*nmol/min/mg*	*nmol/min/mg*	*nmol/min/mg*	%	%
Mouse	10 ± 2	47.5 ± 8	1.8 ± 0.03	1.2 ± 0.08	11 (1 = 11 fold)[c]	2.3 (0.17 = 13 fold)[c]
Rat	35 ± 5	202 ± 38	1.16 ± 0.03	0.55 ± 0.04	2 (0.3 = ~7 fold)[c]	0.25 (0.04 = 6 fold)[c]
Guinea pig	46 ± 2.6	152 ± 8.5	0.56 ± 0.01	0.48 ± 0.06	0.74 (0.2 = ~4 fold)[c]	0.29 (0.04 = 7 fold)[c]

[a]The H_2O_2 emission fluxes reported are those measured in the presence of both inhibitors simultaneously (50 nM AF + 10 μM DNCB).

[b]The numbers shown correspond to the percentage of the O_2 consumption flux diverted to ROS. These values are obtained from calculations using VO_2 and H_2O_2 emission that are in the same units, with the values corrected for the increase in state 4 (60%; Fig. 3 A) and 3 (10%; Fig. 3 B) respiration produced by the presence of AF and DNCB together. For example, in the mouse in state 4 mitochondria, the H_2O_2 emission (=1.8) represents 11% of the O_2 consumption flux (=10 + 6; this latter number is a result of the 60% increase in state 4 respiration, provoked by the presence of both inhibitors simultaneously, i.e., 10 × 0.6 = 6; see Fig. 3 A); thus, 1.8/16 × 100 = 11.2. A similar type of calculation was applied to all other cases.

[c]These values represent the percentage of the respiratory flux diverted to ROS in states 4 and 3 under FET in the absence of inhibitors (see Table 3, Control row).

mouse mitochondria. As an example, in state 4 mouse mitochondria, the H_2O_2 emission in the absence of inhibitors represents 1% of VO_2 (i.e., $10 \times 0.01 = 0.1$ nmol H_2O_2/min/mg protein; when the GSH and Trx systems are both inhibited, the H_2O_2 emission is 1.8 nmol H_2O_2/min/mg protein; thus, 1.8/0.1 = 18-fold increase in H_2O_2 emission). Lower values were detected in the case of guinea pig mitochondria (Table 4). Importantly, in mouse mitochondria, simulation of separate inhibition of TrxR2 (Fig. 5 A) or GR (Fig. 5 B) closely reproduces the shape and magnitude of the dose response of H_2O_2 emission to each one of the inhibitors (Fig. 2 A). A 4- and 19-fold increase in H_2O_2 emission could be simulated, close to the experimentally measured rise of ∼6 and 19 fold at state 4 with AF and DNCB, respectively (Fig. 2 A and Table 3).

Model simulations also showed that H_2O_2 emission is highly dependent on NADPH levels (see Fig. S2). When NADPH decreases below the K_m of GR and TrxR for NADPH (15 and 12 µM, respectively), the antioxidant capacity is quickly exhausted, and higher rates of H_2O_2 emission are observed (Fig. S2 and Table 2).

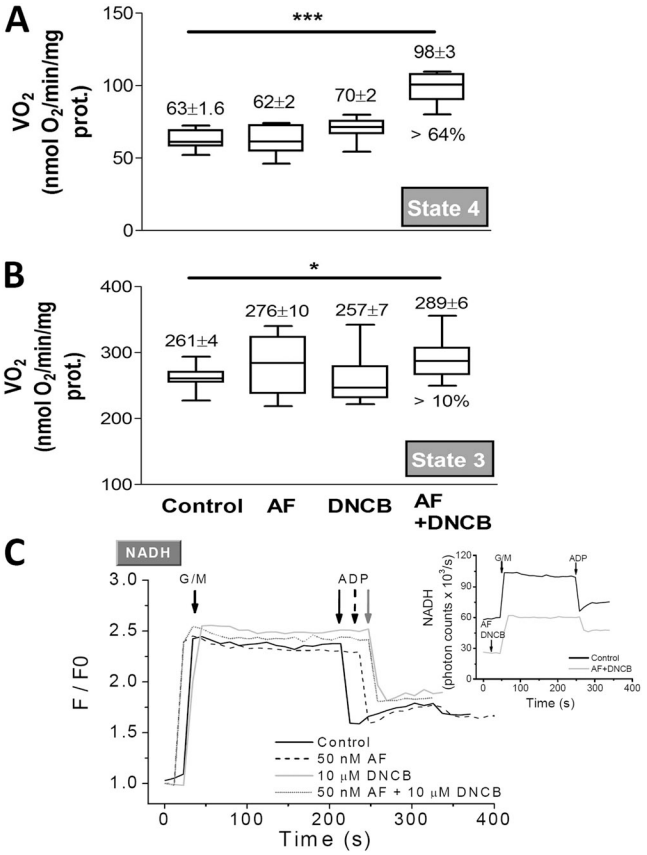

Figure 3. Respiration and redox behavior of mitochondria in the presence of AF and/or DNCB. (A and B) Freshly isolated mitochondria from guinea pig heart were handled and assayed, as described in Materials and methods. Mitochondrial respiration (VO_2) was monitored under FET conditions in state 4 with G/M (A) and state 3 after addition of 1 mM ADP (B) in the absence or the presence of 50 nM AF or 10 µM DNCB or both together. The statistical significance of the differences between treatments was evaluated with ANOVA using Tukey's multiple comparison test (*, $p < 0.05$; ***, $p < 0.001$). (C) The same mitochondrial preparation was analyzed in parallel by fluorometry for NADH and H_2O_2 emission (see Table 4), which were monitored simultaneously after preincubation, with the concentrations of AF and DNCB indicated. Arrows point to substrate (G/M and ADP) addition. In the whisker plots, the top and the bottom of the box represent the 75 and 25% percentile, respectively, whereas the line within the box is the median; the bars indicate the maximum and minimum values of the distribution. The numbers on top of the whisker plots correspond to the mean ± SEM ($n = 12$, with two experiments). prot., protein.

DISCUSSION

In this work, we have addressed the following basic question: how much of the total flux of ROS produced by the respiratory chain is scavenged and, thus, is not accounted for in measurements of H_2O_2 emission from mitochondria? Here, we provide the following answers/observations: (a) the actual electron flux diverted to ROS production rather than O_2 reduction by cytochrome oxidase can be much higher than previously estimated; and (b) the low H_2O_2 emission usually reported during FET is a result of the combined actions of the GSH and Trx1/2 systems, which continuously limit the amount of ROS escaping from mitochondria.

Our quantitative analysis indicates that if the scavenging contribution is not taken into account, the extent of ongoing ROS generation contributed by the respiratory chain is severely underestimated. This evidence is shown in Table 4. For the mouse mitochondria and rat and guinea pig mitochondria, the differences in the ROS rate amount to 11, 7, and 4 fold during state 4 respiration and 13, 6, and 7 fold in state 3 respiration, respectively (Table 4, last two columns).

Earlier measurements in state 4 during FET conducted in mitochondria from rat liver or pigeon heart estimated that the H_2O_2 emission represented ∼1–2% of the total O_2 utilization (Chance et al., 1979). Other authors reported lower values, namely in the range of 0.15–0.6% (see Table 5). Negligible H_2O_2 emission was purported to exist during state 3 respiration, although the levels were not actually determined. Our data indicate values in the range of 0.02–0.04% for mitochondria in state 3 from rat and guinea pig hearts; in the mouse, these values increased ∼10 times (Table 5). Our results point out that, without taking into account the ROS scavenging action, all previous values (including our own data; Aon et al., 2010a) represent underestimations of ROS production from the respiratory chain. The extent of underestimation can be as high as 11 fold in state 4 and 13 fold in state 3 mitochondria from mouse (Table 4). The standard explanation of the observed decrease in ROS emission during the state 4 to state 3 transition is that it results from $\Delta\Psi_m$ depolarization (Schönfeld and Wojtczak, 2008), which is a result of

the activation of ATP synthesis and the concomitant consumption of $\Delta\Psi_m$ by the ATP synthase, leading to an increase in proton pumping and respiration to reestablish the proton-motive force.

The present findings suggest that a large portion of the decrease in ROS emission in state 3 is a result of the action of the GSH and Trx systems, which offset a significant amount of O_2^- production at complex I (e.g., flavin mononucleotide site) or complex III (e.g., ubisemiquinone). At the present stage, we cannot rule out that some unknown fraction of the scavenging systems is not inhibited by the compounds used in this work, which would result in even higher H_2O_2 production rates.

Recently, we showed that AF, an established antirheumatoid gold(I) drug that also exhibits anticancer activity (Rackham et al., 2007; Rigobello et al., 2009), increased H_2O_2 emission from heart mitochondria by selectively inhibiting the TrxR/Trx/Prx system in the nanomolar range (<10 nM; Stanley et al., 2011). Using a similar approach, a very recent study from Kudin et al. (2012) shows the important contribution of the Trx2 system in H_2O_2 detoxification operated by mitochondria in rat hippocampus. Organic gold inhibitors such as AF (Gromer et al., 1998; Zhong et al., 1998) effectively target the selenocysteine of TrxR1 or TrxR2 because selenols bind more efficiently to heavy metals. We assumed that AF was inhibiting TrxR in both matrix and IMS compartments. In the same study, we showed that 2,4-DNCB, an alkylating and GSH-depleting agent (Han et al., 2003), increases H_2O_2 emission, likely through GSH-DNCB conjugation catalyzed by GSH *S*-transferase (Novogrodsky et al., 1979). The inhibitory action of AF and DNCB appeared to be largely independent of one another, influencing H_2O_2 emission only, without substantially affecting mitochondrial energetics ($\Delta\Psi_m$) and the redox status of NADH (Stanley et al., 2011). Notably, the participation of the Trx system is markedly higher than anticipated if one considers that the GSH concentration exceeds Trx by >100 fold. In agreement with previously reported values (Garcia et al., 2010), our measurements in mouse mitochondria indicate that the GSH pool is 1–1.5 mM (Stanley et al., 2011), whereas Trx2 has been estimated to be 10 µM (Cox et al., 2010). Speculatively, this could be explained by a closer localization of the Trx system, relative to GSH, to the sources of ROS in mitochondria.

Previous studies have shown a clear link between GSH depletion and H_2O_2 and O_2^- generation in mitochondria and cells (Han et al., 2003; Aon et al., 2007, 2010a; Stanley et al., 2011). Apparently, in heart mitochondria, a certain degree of GSH depletion (∼30–40%) needs to be attained before a high H_2O_2 emission is manifested (Han et al., 2003). H_2O_2 emission under FET did not increase before overcoming a certain level of GSH

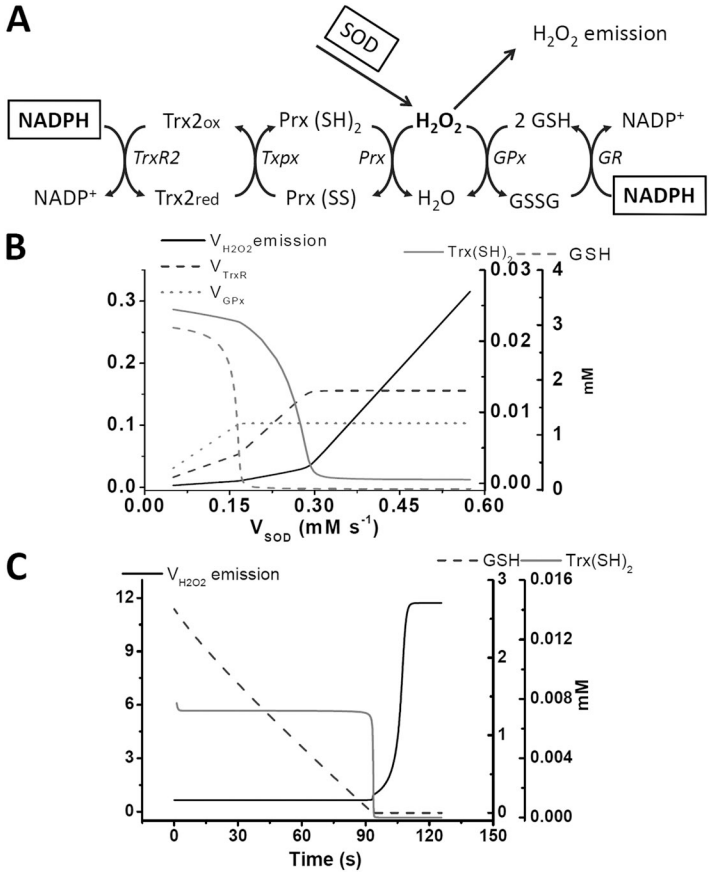

Figure 4. Time-dependent and steady-state behavior of the computational model of GSH/Trx systems. (A) The scheme of the computational model as described in Materials and methods. (B) The continuation analysis of the steady-state behavior as a function of the rate of H_2O_2 provision by SOD activity (V_{SOD}); the latter was varied between 5×10^{-5} and 5.5×10^{-4} mM ms^{-1}, with $k^1_{TrxR} = 0.022$ ms^{-1} and $k^1_{GR} = 0.025$ ms^{-1}. (C) Time-dependent simulations showing the increase in the emission of H_2O_2 upon inhibition of k^1_{TrxR} and k^1_{GR}, which were adjusted from 0.022 to 0.009 ms^{-1} and 0.025 to 0.005 ms^{-1}, respectively, to represent the inhibitory action of AF and DNCB, respectively.

depletion (Han et al., 2003; Aon et al., 2007; Stanley et al., 2011). This behavior is reproduced by our minimal computational model in which the onset of the large increase of H_2O_2 emission occurs only when GSH and $Trx(SH)_2$ levels decrease beyond a certain value (Fig. 4). Our model simulations show that the individual antioxidant systems can relieve each other when the catalytic capacity of either of them is overwhelmed. As a result, the overall function of the scavenging systems is highly dependent on NADPH that, as an electron donor, restores their scavenging ability (Fig. S2). The simulation results also suggest that GSH and Trx systems act interdependently; this interdependence can be not only kinetic but further could involve physical (molecular) interaction among components. In this latter case, inhibition of one system can negatively affect the proper function of the other. This may help to explain the higher fluxes of H_2O_2 emission registered when each system is inhibited independently rather than simultaneously (compare Tables 3 and 4). This interesting aspect is under current investigation in our laboratory.

Several theoretical and pragmatic consequences arise from the findings reported in this work. First and foremost, the two main known antioxidant systems in the mitochondrial matrix work continuously and concertedly to offset ROS produced in the respiratory chain. Second, the H_2O_2 input from the respiratory chain to the scavenging systems is much greater than previously measured. These findings bring to the surface two additional relevant points: (1) the GSH/Trx systems exert a high degree of control over the H_2O_2 emission flux, which modulates the intramitochondrial and -cellular redox environment, and (2) in this context, the respiratory chain and the levels of O_2 acquire a special importance because ROS production represents a relatively higher percentage of the total O_2 consumption flux by mitochondria in comparison with previous estimations. Also, the participation of GSH and Trx systems in H_2O_2 scavenging may differ between different species as herein reported, and this divergence may become even more prominent with other animals of different size. This is an intriguing question to ponder in future studies. Finally, clinical trials testing the impact of antioxidants against acute and chronic cardiac conditions, such as ischemia/reperfusion injury and heart failure, have been rather disappointing, both in terms of functional outcome and prevention of mortality. One obvious explanation could be that some of these antioxidants do not really reach mitochondria, which are increasingly appreciated as a central source of ROS under stressful energetic and redox conditions. Another explanation could be that the maximum rates of reoxidation/recycling of the exogenously added antioxidants limit their effectiveness as compared with the native, finely tuned scavenger pathways. Our study provides a basic mechanistic platform upon which future studies aimed at preventing excessive ROS emission from mitochondria can be designed. In this sense, the strategies of reinforcing the mitochondrial matrix antioxidant defenses appear to be in the right direction (Skulachev et al., 2009; Manczak et al., 2010; Dai et al., 2011; Smith et al., 2011). As has been previously discussed (Jones and Go, 2010), failure of antioxidant therapy might also be a consequence of disruption of redox-dependent signaling pathways that are vital for cells to display normal function (Styskal et al., 2012), for example the well-known effect of ROS to trigger increased expression of antioxidant enzymes via the Nrf2 antioxidant response element (Nguyen et al., 2009).

TABLE 5

Literature survey of H_2O_2 emission and electron flow diversion to ROS under FET in isolated mitochondria from different organs and species

Mitochondria source	Species	H_2O_2 emission		O_2 consumption flux diverted to H_2O_2	Reference
		State 4	State 3	(State 4–State 3)	
		nmol/min/mg protein	*nmol/min/mg protein*	%	
Heart	Rat	0.02	ND	0.4–ND	Hansford et al., 1997
		ndet	ND		St-Pierre et al., 2002
		0.105	0.08	0.3–0.04	This study
	Pigeon	0.3–0.6	ND	2–ND	Chance et al., 1979
		ndet	ND		St-Pierre et al., 2002
	Guinea pig	0.075	0.047	0.6–0.016	Aon et al., 2010a
		0.095	0.062	0.2–0.04	This study
	Mouse	0.107	0.082	1–0.17	This study
Liver	Rat	0.19	0.08	1-2–ND	Boveris et al., 1972
		0.25	ND	1.82–ND	Hoffman and Brookes, 2009
Skeletal muscle	Rat	<0.2	ND	≤0.15–ND	St-Pierre et al., 2002

In all sources, FET is under G/M or Pyr/M (4–6 mM each). The only exception is St-Pierre et al. (2002), in which the data reported in the table were obtained with palmitoyl carnitine. ndet, non-detected.

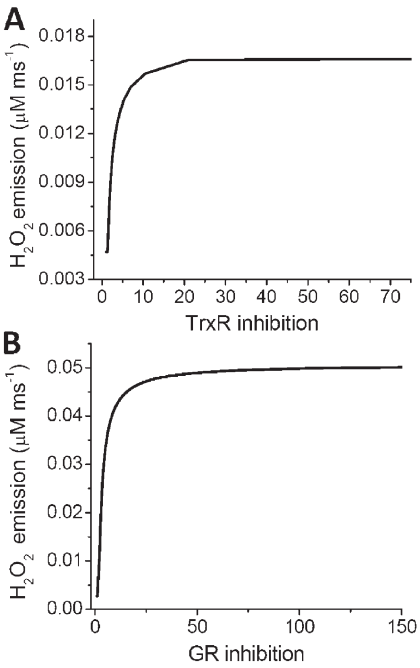

Figure 5. Model simulation of mitochondrial H_2O_2 emission after independent inhibition of Trx or GSH system. (A) To simulate AF inhibition with the computational model, the concentration of TrxR2 (Etrxm) was decreased from a control concentration of 0.002 to 10^{-8} mM. The steady-state values of H_2O_2 emission were estimated for each concentration at fixed GR (kcgrm = 0.0152). (B) DNCB inhibition was simulated by decreasing the concentration of GR (kcgrm) from a control value of 0.0215 mM to 10^{-8} mM and the steady-state values of H_2O_2 emission estimated at each concentration while keeping TrxR2 constant (Etrxm = 0.0035). In both cases, the percentage of inhibition was calculated by dividing the control concentration over the corresponding TrxR2 or GR concentration. The parameters used in this simulation were kcgpx = 0.013 mM, $V_{SOD} = 8 \times 10^{-5}$ mM ms^{-1}, kpxx = 2.5 mM, and Prx3T = 0.5 mM.

Overall, the present findings reinforce the idea that mitochondria and their bacterial precursors, emerging at the dawn of aerobic life, have evolved powerful antioxidant systems whose coordinated actions continuously keep ROS levels within physiological limits to avoid oxidative damage while ensuring the preservation of vital signaling pathways and maximal energy output.

This work was supported by National Institutes of Health grants R21HL106054 (to S. Cortassa), R01-HL091923-01 (to M.A. Aon and N. Paolocci), R37-HL54598 (to B. O'Rourke), and P01HL107153 (to N. Paolocci). An American Heart Association postdoctoral fellowship grant 10POST414001 to B.A. Stanley supported him, and a diversity supplement R01-HL091923-01 from the National Heart, Lung, and Blood Institute Diversity Supplement Program to J.M. Kembro supported her.

Angus C. Nairn served as editor.

Submitted: 11 January 2012
Accepted: 24 April 2012

REFERENCES

Adam-Vizi, V., and C. Chinopoulos. 2006. Bioenergetics and the formation of mitochondrial reactive oxygen species. *Trends Pharmacol. Sci.* 27:639–645. http://dx.doi.org/10.1016/j.tips.2006.10.005

Adimora, N.J., D.P. Jones, and M.L. Kemp. 2010. A model of redox kinetics implicates the thiol proteome in cellular hydrogen peroxide responses. *Antioxid. Redox Signal.* 13:731–743. http://dx.doi.org/10.1089/ars.2009.2968

Andreyev, A.Y., Y.E. Kushnareva, and A.A. Starkov. 2005. Mitochondrial metabolism of reactive oxygen species. *Biochemistry (Mosc.).* 70:200–214. http://dx.doi.org/10.1007/s10541-005-0102-7

Aon, M.A., S. Cortassa, F.G. Akar, and B. O'Rourke. 2006. Mitochondrial criticality: A new concept at the turning point of life or death. *Biochim. Biophys. Acta.* 1762:232–240.

Aon, M.A., S. Cortassa, C. Maack, and B. O'Rourke. 2007. Sequential opening of mitochondrial ion channels as a function of glutathione redox thiol status. *J. Biol. Chem.* 282:21889–21900. http://dx.doi.org/10.1074/jbc.M702841200

Aon, M.A., S. Cortassa, F.G. Akar, D.A. Brown, L. Zhou, and B. O'Rourke. 2009. From mitochondrial dynamics to arrhythmias. *Int. J. Biochem. Cell Biol.* 41:1940–1948. http://dx.doi.org/10.1016/j.biocel.2009.02.016

Aon, M.A., S. Cortassa, and B. O'Rourke. 2010a. Redox-optimized ROS balance: A unifying hypothesis. *Biochim. Biophys. Acta.* 1797:865–877. http://dx.doi.org/10.1016/j.bbabio.2010.02.016

Aon, M.A., S. Cortassa, A.C. Wei, M. Grunnet, and B. O'Rourke. 2010b. Energetic performance is improved by specific activation of K+ fluxes through K(Ca) channels in heart mitochondria. *Biochim. Biophys. Acta.* 1797:71–80.

Balaban, R.S., S. Nemoto, and T. Finkel. 2005. Mitochondria, oxidants, and aging. *Cell.* 120:483–495. http://dx.doi.org/10.1016/j.cell.2005.02.001

Barja, G. 1998. Mitochondrial free radical production and aging in mammals and birds. *Ann. NY Acad. Sci.* 854:224–238. http://dx.doi.org/10.1111/j.1749-6632.1998.tb09905.x

Bedard, K., and K.H. Krause. 2007. The NOX family of ROS-generating NADPH oxidases: Physiology and pathophysiology. *Physiol. Rev.* 87:245–313. http://dx.doi.org/10.1152/physrev.00044.2005

Biary, N., C. Xie, J. Kauffman, and F.G. Akar. 2011. Biophysical properties and functional consequences of reactive oxygen species (ROS)-induced ROS release in intact myocardium. *J. Physiol.* 589:5167–5179.

Boveris, A., N. Oshino, and B. Chance. 1972. The cellular production of hydrogen peroxide. *Biochem. J.* 128:617–630.

Brown, D.A., M.A. Aon, C.R. Frasier, R.C. Sloan, A.H. Maloney, E.J. Anderson, and B. O'Rourke. 2010. Cardiac arrhythmias induced by glutathione oxidation can be inhibited by preventing mitochondrial depolarization. *J. Mol. Cell. Cardiol.* 48:673–679. http://dx.doi.org/10.1016/j.yjmcc.2009.11.011

Butler, J., W.H. Koppenol, and E. Margoliash. 1982. Kinetics and mechanism of the reduction of ferricytochrome c by the superoxide anion. *J. Biol. Chem.* 257:10747–10750.

Camara, A.K., M. Bienengraeber, and D.F. Stowe. 2011. Mitochondrial approaches to protect against cardiac ischemia and reperfusion injury. *Front Physiol.* 2:13. http://dx.doi.org/10.3389/fphys.2011.00013

Chance, B., H. Sies, and A. Boveris. 1979. Hydroperoxide metabolism in mammalian organs. *Physiol. Rev.* 59:527–605.

Chockalingam, K., J. Luba, H.S. Nick, D.N. Silverman, and H. Zhao. 2006. Engineering and characterization of human manganese superoxide dismutase mutants with high activity and low product inhibition. *FEBS J.* 273:4853–4861. http://dx.doi.org/10.1111/j.1742-4658.2006.05484.x

Cortassa, S., M.A. Aon, R.L. Winslow, and B. O'Rourke. 2004. A mitochondrial oscillator dependent on reactive oxygen species. *Biophys. J.* 87:2060–2073. http://dx.doi.org/10.1529/biophysj.104.041749

Cox, A.G., C.C. Winterbourn, and M.B. Hampton. 2010. Mitochondrial peroxiredoxin involvement in antioxidant defence and redox signalling. *Biochem. J.* 425:313–325. http://dx.doi.org/10.1042/BJ20091541

Dai, D.F., S.C. Johnson, J.J. Villarin, M.T. Chin, M. Nieves-Cintrón, T. Chen, D.J. Marcinek, G.W. Dorn II, Y.J. Kang, T.A. Prolla, et al. 2011. Mitochondrial oxidative stress mediates angiotensin II-induced cardiac hypertrophy and Galphaq overexpression-induced heart failure. *Circ. Res.* 108:837–846. http://dx.doi.org/10.1161/CIRCRESAHA.110.232306

Dhooge, A., W. Govaerts, Yu.A. Kuznetsov, H.G.E. Meijer, and B. Sautois. 2008. New features of the software MATCONT for bifurcation analysis of dynamical systems. *Math. Comput. Model. Dyn. Syst.* 14:147–175. http://dx.doi.org/10.1080/13873950701742754

Drechsel, D.A., and M. Patel. 2010. Respiration-dependent H2O2 removal in brain mitochondria via the thioredoxin/peroxiredoxin system. *J. Biol. Chem.* 285:27850–27858. http://dx.doi.org/10.1074/jbc.M110.101196

Eckenroth, B., K. Harris, A.A. Turanov, V.N. Gladyshev, R.T. Raines, and R.J. Hondal. 2006. Semisynthesis and characterization of mammalian thioredoxin reductase. *Biochemistry.* 45:5158–5170. http://dx.doi.org/10.1021/bi0517887

Garcia, J., D. Han, H. Sancheti, L.P. Yap, N. Kaplowitz, and E. Cadenas. 2010. Regulation of mitochondrial glutathione redox status and protein glutathionylation by respiratory substrates. *J. Biol. Chem.* 285:39646–39654. http://dx.doi.org/10.1074/jbc.M110.164160

Go, Y.-M., and D.P. Jones. 2008. Redox compartmentalization in eukaryotic cells. *Biochim. Biophys. Acta.* 1780:1273–1290. http://dx.doi.org/10.1016/j.bbagen.2008.01.011

Gromer, S., L.D. Arscott, C.H. Williams Jr., R.H. Schirmer, and K. Becker. 1998. Human placenta thioredoxin reductase. Isolation of the selenoenzyme, steady state kinetics, and inhibition by therapeutic gold compounds. *J. Biol. Chem.* 273:20096–20101. http://dx.doi.org/10.1074/jbc.273.32.20096

Han, D., E. Williams, and E. Cadenas. 2001. Mitochondrial respiratory chain-dependent generation of superoxide anion and its release into the intermembrane space. *Biochem. J.* 353:411–416. http://dx.doi.org/10.1042/0264-6021:3530411

Han, D., R. Canali, D. Rettori, and N. Kaplowitz. 2003. Effect of glutathione depletion on sites and topology of superoxide and hydrogen peroxide production in mitochondria. *Mol. Pharmacol.* 64:1136–1144. http://dx.doi.org/10.1124/mol.64.5.1136

Hansford, R.G., B.A. Hogue, and V. Mildaziene. 1997. Dependence of H2O2 formation by rat heart mitochondria on substrate availability and donor age. *J. Bioenerg. Biomembr.* 29:89–95. http://dx.doi.org/10.1023/A:1022420007908

Hoffman, D.L., and P.S. Brookes. 2009. Oxygen sensitivity of mitochondrial reactive oxygen species generation depends on metabolic conditions. *J. Biol. Chem.* 284:16236–16245. http://dx.doi.org/10.1074/jbc.M809512200

Holmgren, A., and J. Lu. 2010. Thioredoxin and thioredoxin reductase: Current research with special reference to human disease. *Biochem. Biophys. Res. Commun.* 396:120–124. http://dx.doi.org/10.1016/j.bbrc.2010.03.083

Hu, J., L. Dong, and C.E. Outten. 2008. The redox environment in the mitochondrial intermembrane space is maintained separately from the cytosol and matrix. *J. Biol. Chem.* 283:29126–29134. http://dx.doi.org/10.1074/jbc.M803028200

Imai, H., and Y. Nakagawa. 2003. Biological significance of phospholipid hydroperoxide glutathione peroxidase (PHGPx, GPx4) in mammalian cells. *Free Radic. Biol. Med.* 34:145–169. http://dx.doi.org/10.1016/S0891-5849(02)01197-8

Iñarrea, P., H. Moini, D. Han, D. Rettori, I. Aguiló, M.A. Alava, M. Iturralde, and E. Cadenas. 2007. Mitochondrial respiratory chain and thioredoxin reductase regulate intermembrane Cu,Zn-superoxide dismutase activity: Implications for mitochondrial energy metabolism and apoptosis. *Biochem. J.* 405:173–179.

Jones, D.P., and Y.M. Go. 2010. Redox compartmentalization and cellular stress. *Diabetes Obes. Metab.* 12(Suppl 2):116–125. http://dx.doi.org/10.1111/j.1463-1326.2010.01266.x

Kaludercic, N., E. Takimoto, T. Nagayama, N. Feng, E.W. Lai, D. Bedja, K. Chen, K.L. Gabrielson, R.D. Blakely, J.C. Shih, et al. 2010. Monoamine oxidase A-mediated enhanced catabolism of norepinephrine contributes to adverse remodeling and pump failure in hearts with pressure overload. *Circ. Res.* 106:193–202. http://dx.doi.org/10.1161/CIRCRESAHA.109.198366

Korshunov, S.S., B.F. Krasnikov, M.O. Pereverzev, and V.P. Skulachev. 1999. The antioxidant functions of cytochrome c. *FEBS Lett.* 462:192–198. http://dx.doi.org/10.1016/S0014-5793(99)01525-2

Kowaltowski, A.J., N.C. de Souza-Pinto, R.F. Castilho, and A.E. Vercesi. 2009. Mitochondria and reactive oxygen species. *Free Radic. Biol. Med.* 47:333–343. http://dx.doi.org/10.1016/j.freeradbiomed.2009.05.004

Kudin, A.P., B. Augustynek, A.K. Lehmann, R. Kovács, and W.S. Kunz. 2012. The contribution of thioredoxin-2 reductase and glutathione peroxidase to H(2)O(2) detoxification of rat brain mitochondria. *Biochim. Biophys. Acta.* In press.

Kuroda, J., T. Ago, S. Matsushima, P. Zhai, M.D. Schneider, and J. Sadoshima. 2010. NADPH oxidase 4 (Nox4) is a major source of oxidative stress in the failing heart. *Proc. Natl. Acad. Sci. USA.* 107:15565–15570. http://dx.doi.org/10.1073/pnas.1002178107

Manczak, M., P. Mao, M.J. Calkins, A. Cornea, A.P. Reddy, M.P. Murphy, H.H. Szeto, B. Park, and P.H. Reddy. 2010. Mitochondria-targeted antioxidants protect against amyloid-beta toxicity in Alzheimer's disease neurons. *J. Alzheimers Dis.* 20:S609–S631.

Murphy, M.P. 2009. How mitochondria produce reactive oxygen species. *Biochem. J.* 417:1–13. http://dx.doi.org/10.1042/BJ20081386

Nguyen, T., P. Nioi, and C.B. Pickett. 2009. The Nrf2-antioxidant response element signaling pathway and its activation by oxidative stress. *J. Biol. Chem.* 284:13291–13295. http://dx.doi.org/10.1074/jbc.R900010200

Novogrodsky, A., R.E. Nehring Jr., and A. Meister. 1979. Inhibition of amino acid transport into lymphoid cells by the glutamine analog L-2-amino-4-oxo-5-chloropentanoate. *Proc. Natl. Acad. Sci. USA.* 76:4932–4935. http://dx.doi.org/10.1073/pnas.76.10.4932

Pasdois, P., J.E. Parker, E.J. Griffiths, and A.P. Halestrap. 2011. The role of oxidized cytochrome c in regulating mitochondrial reactive oxygen species production and its perturbation in ischaemia. *Biochem. J.* 436:493–505. http://dx.doi.org/10.1042/BJ20101957

Pereverzev, M.O., T.V. Vygodina, A.A. Konstantinov, and V.P. Skulachev. 2003. Cytochrome c, an ideal antioxidant. *Biochem. Soc. Trans.* 31:1312–1315. http://dx.doi.org/10.1042/BST0311312

Pérez, V.I., C.M. Lew, L.A. Cortez, C.R. Webb, M. Rodriguez, Y. Liu, W. Qi, Y. Li, A. Chaudhuri, H. Van Remmen, et al. 2008. Thioredoxin 2 haploinsufficiency in mice results in impaired mitochondrial function and increased oxidative stress. *Free Radic. Biol. Med.* 44:882–892. http://dx.doi.org/10.1016/j.freeradbiomed.2007.11.018

Pillay, C.S., J.H. Hofmeyr, B.G. Olivier, J.L. Snoep, and J.M. Rohwer. 2009. Enzymes or redox couples? The kinetics of thioredoxin and

glutaredoxin reactions in a systems biology context. *Biochem. J.* 417:269–275. http://dx.doi.org/10.1042/BJ20080690

Rackham, O., S.J. Nichols, P.J. Leedman, S.J. Berners-Price, and A. Filipovska. 2007. A gold(I) phosphine complex selectively induces apoptosis in breast cancer cells: Implications for anticancer therapeutics targeted to mitochondria. *Biochem. Pharmacol.* 74:992–1002. http://dx.doi.org/10.1016/j.bcp.2007.07.022

Radi, R., J.F. Turrens, L.Y. Chang, K.M. Bush, J.D. Crapo, and B.A. Freeman. 1991. Detection of catalase in rat heart mitochondria. *J. Biol. Chem.* 266:22028–22034.

Rhee, S.G., S.W. Kang, T.S. Chang, W. Jeong, and K. Kim. 2001. Peroxiredoxin, a novel family of peroxidases. *IUBMB Life.* 52:35–41. http://dx.doi.org/10.1080/15216540252774748

Rigobello, M.P., V. Gandin, A. Folda, A.K. Rundlöf, A.P. Fernandes, A. Bindoli, C. Marzano, and M. Björnstedt. 2009. Treatment of human cancer cells with selenite or tellurite in combination with auranofin enhances cell death due to redox shift. *Free Radic. Biol. Med.* 47:710–721. http://dx.doi.org/10.1016/j.freeradbiomed.2009.05.027

Rydström, J. 2006. Mitochondrial transhydrogenase—a key enzyme in insulin secretion and, potentially, diabetes. *Trends Biochem. Sci.* 31:355–358. http://dx.doi.org/10.1016/j.tibs.2006.05.003

Salvi, M., V. Battaglia, A.M. Brunati, N. La Rocca, E. Tibaldi, P. Pietrangeli, L. Marcocci, B. Mondovì, C.A. Rossi, and A. Toninello. 2007. Catalase takes part in rat liver mitochondria oxidative stress defense. *J. Biol. Chem.* 282:24407–24415. http://dx.doi.org/10.1074/jbc.M701589200

Sanz, A., G. Barja, R. Pamplona, and C. Leeuwenburgh. 2009. Free Radicals and Mammalian Aging. *In* Redox Signaling and Regulation in Biology and Medicine. C. Jacob and P.G. Winyard, editors. Wiley-VCH GmbH & Co., Weinheim, Germany. 433–472.

Sazanov, L.A., and J.B. Jackson. 1994. Proton-translocating transhydrogenase and NAD- and NADP-linked isocitrate dehydrogenases operate in a substrate cycle which contributes to fine regulation of the tricarboxylic acid cycle activity in mitochondria. *FEBS Lett.* 344:109–116. http://dx.doi.org/10.1016/0014-5793(94)00370-X

Schönfeld, P., and L. Wojtczak. 2008. Fatty acids as modulators of the cellular production of reactive oxygen species. *Free Radic. Biol. Med.* 45:231–241. http://dx.doi.org/10.1016/j.freeradbiomed.2008.04.029

Sheeran, F.L., J. Rydström, M.I. Shakhparonov, N.B. Pestov, and S. Pepe. 2010. Diminished NADPH transhydrogenase activity and mitochondrial redox regulation in human failing myocardium. *Biochim. Biophys. Acta.* 1797:1138–1148. http://dx.doi.org/10.1016/j.bbabio.2010.04.002

Skulachev, V.P., V.N. Anisimov, Y.N. Antonenko, L.E. Bakeeva, B.V. Chernyak, V.P. Erichev, O.F. Filenko, N.I. Kalinina, V.I. Kapelko, N.G. Kolosova, et al. 2009. An attempt to prevent senescence: A mitochondrial approach. *Biochim. Biophys. Acta.* 1787:437–461. http://dx.doi.org/10.1016/j.bbabio.2008.12.008

Slodzinski, M.K., M.A. Aon, and B. O'Rourke. 2008. Glutathione oxidation as a trigger of mitochondrial depolarization and oscillation in intact hearts. *J. Mol. Cell. Cardiol.* 45:650–660. http://dx.doi.org/10.1016/j.yjmcc.2008.07.017

Smith, R.A., R.C. Hartley, and M.P. Murphy. 2011. Mitochondria-targeted small molecule therapeutics and probes. *Antioxid. Redox Signal.* 15:3021–3038. http://dx.doi.org/10.1089/ars.2011.3969

Stanley, B.A., V. Sivakumaran, S. Shi, I. McDonald, D. Lloyd, W.H. Watson, M.A. Aon, and N. Paolocci. 2011. Thioredoxin reductase-2 is essential for keeping low levels of H(2)O(2) emission from isolated heart mitochondria. *J. Biol. Chem.* 286:33669–33677. http://dx.doi.org/10.1074/jbc.M111.284612

Starkov, A.A., G. Fiskum, C. Chinopoulos, B.J. Lorenzo, S.E. Browne, M.S. Patel, and M.F. Beal. 2004. Mitochondrial alpha-ketoglutarate dehydrogenase complex generates reactive oxygen species. *J. Neurosci.* 24:7779–7788. http://dx.doi.org/10.1523/JNEUROSCI.1899-04.2004

Stowe, D.F., and A.K. Camara. 2009. Mitochondrial reactive oxygen species production in excitable cells: Modulators of mitochondrial and cell function. *Antioxid. Redox Signal.* 11:1373–1414. http://dx.doi.org/10.1089/ars.2008.2331

St-Pierre, J., J.A. Buckingham, S.J. Roebuck, and M.D. Brand. 2002. Topology of superoxide production from different sites in the mitochondrial electron transport chain. *J. Biol. Chem.* 277:44784–44790. http://dx.doi.org/10.1074/jbc.M207217200

Styskal, J., H. Van Remmen, A. Richardson, and A.B. Salmon. 2012. Oxidative stress and diabetes: What can we learn about insulin resistance from antioxidant mutant mouse models? *Free Radic. Biol. Med.* 52:46–58. http://dx.doi.org/10.1016/j.freeradbiomed.2011.10.441

Sztajer, H., B. Gamain, K.D. Aumann, C. Slomianny, K. Becker, R. Brigelius-Flohé, and L. Flohé. 2001. The putative glutathione peroxidase gene of Plasmodium falciparum codes for a thioredoxin peroxidase. *J. Biol. Chem.* 276:7397–7403. http://dx.doi.org/10.1074/jbc.M008631200

Zhong, L., E.S. Arnér, J. Ljung, F. Aslund, and A. Holmgren. 1998. Rat and calf thioredoxin reductase are homologous to glutathione reductase with a carboxyl-terminal elongation containing a conserved catalytically active penultimate selenocysteine residue. *J. Biol. Chem.* 273:8581–8591. http://dx.doi.org/10.1074/jbc.273.15.8581